Current **A**pplied **S**cience and **T**echnology e-ISSN: 2586-9396

Curr. Appl. Sci. Technol. ….., Vol... (No...), e0268047

Research article

Acido-alcoholyzed Products of Polylactide (PLA) and Their Use in Enhancing Mechanical Properties, Hydrophilicity, and Cell Compatibility of PLA Nanofibers for Tissue Engineering Applications

Pattara Somnuake[1], Atitsa Petchsuk[2], Mantana Opaprakasit[3] and Pakorn Opaprakasit[1]*

[1]School of Integrated Science and Innovation, Sirindhorn International Institute of Technology (SIIT), Thammasat University, Pathum Thani, 12120, Thailand
[2]National Metal and Materials Technology Center, 114 Thailand Science Park, Pathum Thani, 12120, Thailand
[3]Department of Materials Science, Faculty of Science, Chulalongkorn University, Bangkok, 10330, Thailand

Received: 2 July 2025, Revised: 11 September 2025, Accepted: 26 September 2025, Published: 17 February 2026

Abstract

Alcoholysis and acidolysis effectively transesterify polylactide (PLA) resin into small or medium-sized lactate oligomers with tunable hydrophilicity. The products can then be used to prepare various functional materials. This work employed 2, 2-bis(hydroxymethyl) propionic acid (DMPA) to generate small-sized PLA oligomers with carboxylic and hydroxyl terminals. The chemical structures and compositions of the acido-alcoholyzed PLA (aPLA) were analyzed by proton nuclear magnetic resonance (^{1}H-NMR) and Fourier transform infrared (FTIR) spectroscopy. The optimum product was blended with PLA resin and fabricated into electrospun nanofibers to increase their mechanical properties, hydrophilicity, and biocompatibility. The surface morphology, chemical structures, crystallinity, and properties of the PLA/aPLA blends were characterized by scanning electron microscopy (SEM), FTIR, X-ray diffraction (XRD) spectroscopy, water contact angle (WCA) measurements, tensile tests, and biocompatibility tests. Nanofibers with a ragged surface morphology and a 900-1500 nm size range were generated. The fibers showed higher crystallinity due to the enhanced crystallization induction by the acid and hydroxyl chain ends. Incorporating aPLA increased the elongation at break and the toughness of the fiber mats due to the plasticizing effect and the higher compatibility of aPLA in the PLA matrix. The hydrophilicity of the fiber mats also improved due to the higher contents of the polar end groups, leading to high water absorption in a short time. The cell compatibility results confirmed that the fibers containing 20% aPLAs were suitable for incubating L929 fibroblast cells, which was reflected in the higher adhesion and growth on the cells on the fiber mats within 7 days. The materials have high potential for use in tissue engineering scaffolding and biomedical applications.

Keywords: polylactide; alcoholysis; electrospun nanofibers; tissue engineering

*Corresponding author: E-mail: pakorn@siit.tu.ac.th
https://doi.org/10.55003/cast.2026.268047

1. Introduction

Materials with hydrophilic surfaces and water absorption capability are of interest in biomedical applications, particularly tissue engineering. The optimal material must possess high hydrophilicity to accommodate cell attachment and demonstrate biocompatibility by minimizing cytotoxic effects related to acidity, protein production, and oxidative stress. Various processing techniques have been developed to address these requirements, including functionalized particle synthesis, film casting, 3D printing, and electrospinning. Electrospinning has emerged as a versatile method for creating nanofibers, enabling the effective loading and transportation of critical cellular components such as genes, medications, proteins, and peptides (Bhardwaj & Kundu, 2010). The fundamental principle of electrospinning involves applying a strong electrostatic field to a polymer solution or melt. The electrostatic repulsion within the charged solution overcomes the surface tension and forms a Taylor cone structure, leading to thin liquid jets exploding. As these polymer jets cross through the air toward a grounded collector, the solvent evaporates, and the stretching forces cause the formation of small-sized fibers, ultimately resulting in solid nanofibers deposited on the collector surface. The fabrication process critically depends on multiple parameters, including solution concentration, viscosity, polymer molecular weight, needle-to-collector distance, solvent properties, ambient humidity, and temperature, collectively influencing fiber morphology and overall material performance (Deitzel et al., 2001; Casasola et al., 2014; Kim et al., 2016; Haider et al., 2018; Huang & Thomas, 2018; Promnil et al., 2021). Tissue engineering scaffolds benefit from nanofiber materials whose various functional groups facilitate cell attachment, provide protein binding sites, possess surface modification potential, and control hydrophilicity/hydrophobicity (Somnuake, 2021).

Polylactide (PLA) is a degradable and biocompatible polyester widely applied for electrospinning fabrication. The material is derived from renewable agricultural sources, e.g., corn, sugar cane, and cassava. PLA displays excellent properties, including significant mechanical strength, high optical transparency, and controlled degradability, i.e., converting to naturally metabolized lactic acid (Somnuake et al., 2024a). These properties make PLA ideal for creating high-performance electrospun nanofibers (Pang et al., 2010; Wacharawichanant et al., 2018; Hortos et al., 2019). Recent works investigated the modification of PLA chemical structures, such as branched, grafted, or block structures. Incorporating polar functional groups into the polymer chains can also improve their hydrophilicity, making them better suitable for biomedical use. Transesterification, such as acidolysis and alcoholysis, leads to smaller-sized lactate oligomers with higher hydrophilic end-group compositions, referred to as the sizing down approach (López-Fonseca et al., 2010; Sinha et al., 2010). Alcoholysis presents a promising PLA modification approach, leveraging hydroxyl active groups from diverse diols or polyols (Nim et al., 2020). Microwave-assisted reactions have proven particularly efficient in this process, enabling rapid reaction times, reduced energy consumption, and precise product control. PLA's ester bonds undergo transesterification when diols or polyols are employed, generating smaller lactate oligomers with hydroxyl terminals (Pang et al., 2010; Nim et al., 2020; Nim & Opaprakasit, 2021). In addition, multi-functional reagents, e.g., 2,2-bis hydroxymethyl propionic acid (DMPA), have been used in alcoholyzed and acidolyzed PLA, as these contain multiple hydrophilic groups of carboxylic acid and hydroxyl functional groups. Lactate oligomer products possess two hydroxyls and carboxylic acid terminals, which can be further deprotonated to yield a negative charge for carboxylate (Fuensanta et al., 2020). This size-reduction procedure for creating functionalized PLA oligomers offers significant

advantages over bottom-up synthesis, including lower production costs, shortened reaction times, and enhanced structural directness, expanding potential applications in food-contact, cosmetic, and biomedical applications (Petchsuk et al., 2014; Nim et al., 2023).

After the alcoholysis process, chain scission reactions increase the polar end group content. These functional groups are necessary for interacting with active compounds and drugs, and cell adherence (Benhabbour et al., 2008). The surface's hydrophilicity/hydrophobicity also plays a key role in the performance of biomedical materials. This is commonly characterized by surface wettability, i.e., water contact angle (WCA) (Drelich et al., 2011). According to their WCA value, materials are categorized as hydrophilic (lower than 90°), hydrophobic (between 90 and 150°), and superhydrophobic (higher than 150°). In biomedical applications, these surface characteristics have a significant impact on the material performance and biological interactions, especially nanofibers for cell scaffolds and wound dressings (Shafrin & Zisman, 1960; Ganesan et al., 2016; Wang et al., 2017).

In this work, hydrophilic PLA nanofibers were fabricated by an electrospinning process from the blends of acido-alcoholyzed PLA (aPLA) products derived from the transesterification of PLA by DMPA and a neat PLA matrix. The microwave-assisted acido-alcoholysis generates lactate oligomers with hydroxyl and carboxylic acid end groups. The chemical structures, molecular weight, crystallinity, and thermal properties of the resulting aPLAs were examined. The aPLA product was blended with PLA resin at various ratios to fabricate nanofibers. The resulting nanofibers' morphology, functional groups, surface wettability, and mechanical and thermal properties were analyzed. The cell compatibility of the nanofibers was investigated to assess their potential use in tissue engineering applications.

2. Materials and Methods

2.1 Materials

Polylactide (PLA) 4043D (Mw 200,000 g/mol) was purchased from NatureWorks. 2,2-bis(hydroxymethyl)propionic acid (DMPA) (98%) was obtained from Acros Organics. Chloroform (CHL) and dimethylformamide (DMF) were supplied by VWR Prolabo Chemicals and Carlo Erba. All chemicals were used without further purification.

2.2 Acido-alcoholysis of PLA

PLA resin was transesterified into medium-sized lactate oligomers with carboxylic acid and hydroxyl groups of DMPA, producing acido-alcoholyzed PLA (aPLA) products. The reaction was conducted for 15 min at 190°C under self-developed pressure in a microwave reactor (Discover SP series, CEM Mattews NC, USA). The PLA/DMPA ratio was varied at 6:1 and 12:1 w/w. The aPLA products were then dried overnight at 60°C in an oven for further use.

2.3 Fabrication of electrospun nanofibers

The blend solution of neat PLA resin and aPLA was prepared by separately dissolving each component in a 7:1 v/v CHL/DMF mixed solvent. The solutions were mixed at PLA: aPLA ratios of 80:20 and 50:50, called PLA/aPLA20 and PLA/aPLA50, respectively. The mixtures were stirred for 5 h at 40–50°C, whose solid contents were adjusted at an optimum

concentration for electrospinning (10% w/v for neat PLA, 12% w/v for PLA/aPLA20, and 19% w/v for PLA/aPLA50). A 20 kV high-voltage generator, an aluminum plate collector, a syringe pump, and a needle injector feed system were then used to electrospin the solutions at a flow rate of 5 mL/h. The distance between the needle tip and the collector was 15 cm. The resulting PLA/aPLA fiber mats were collected and dried in an oven at 60°C overnight to remove any remaining solvents.

2.4 Characterization

The chemical structures of the aPLA products were characterized by proton nuclear magnetic resonance (^{1}H-NMR) spectroscopy on an Ascend TM 600/Advance III HD Bruker (Switzerland). The surface morphology of the nanofibers was examined by a scanning electron microscope (FE-SEM) (JSM-6000 Plus, JEOL, Japan). The chemical structures, interactions, and crystalline characteristics of the samples were characterized by Fourier transform infrared (FTIR) spectroscopy in the attenuated total reflectance (ATR) and transmission modes on a Nicolet iS5 spectrometer (Thermo Scientific, USA). The spectra were measured by co-adding 32 scans at a resolution of 4 cm^{-1}. X-ray diffraction (XRD) was evaluated on a Bruker AXS (Model D8 Advance, Germany) with Cu-Kα radiation. The X-ray diffractograms were recorded from 5-40° at 50 kV, 300 mA, with increment of 0.02 degrees/step, and time step 0.4 s^{-1}, using LYNXEYE XE-T as a detector. The mechanical properties of the fiber mat samples were examined in tensile mode on a Tinius Olsen H5KT machine with a 100 N load cell. The nanofiber mat specimens were prepared at ~10 mm in width. The tensile measurements were conducted at a 50 mm gauge length at a speed of 5 mm/min. Each sample was measured in triplicate, and the average and standard deviation values were reported.

The hydrophilicity of the fiber mat samples was measured in terms of water contact angle (WCA) using Dinolite Capture 2.0 software (Dino-Lite & Dino-Eye), employing 20 µL deionized water droplets. The ImageJ program was utilized to calculate the WCA values. Biocompatibility tests were used to observe the cell adhesion ability and biocompatibility of the neat PLA and PLA/aPLA20 nanofibers. MEM complemented medium, supplemented with horse serum and antibiotics, was used. The pH of the medium was maintained in a range of 7.2-7.4. The nanofiber mats were sterilized in an autoclave at 121°C for 15 min before testing. The samples were placed in a 24-well plate. L929 cells (2×10^4 cells) were seeded on the samples and incubated at 37±1°C, 5±0.1% CO_2, and 95±5% relative humidity for 7 days. After that, the samples were fixed with a fixative solution overnight. After the fixation step, dehydration was performed by sequential immersion of samples in ethanol and placing them in an automated critical point dryer. The samples were coated with gold for FE-SEM analysis.

3. Results and Discussion

3.1 Chemical structures of aPLA products

^{1}H-NMR spectra of aPLA products obtained at PLA: DMPA ratios of 6:1 and 12:1, denoted as aPLA61 and aPLA121, and their signal assignments are illustrated in Figure 1(a). Depending on the number of hydroxyls and carboxylic acids involved in the transesterification, the products with three possible structures were generated:

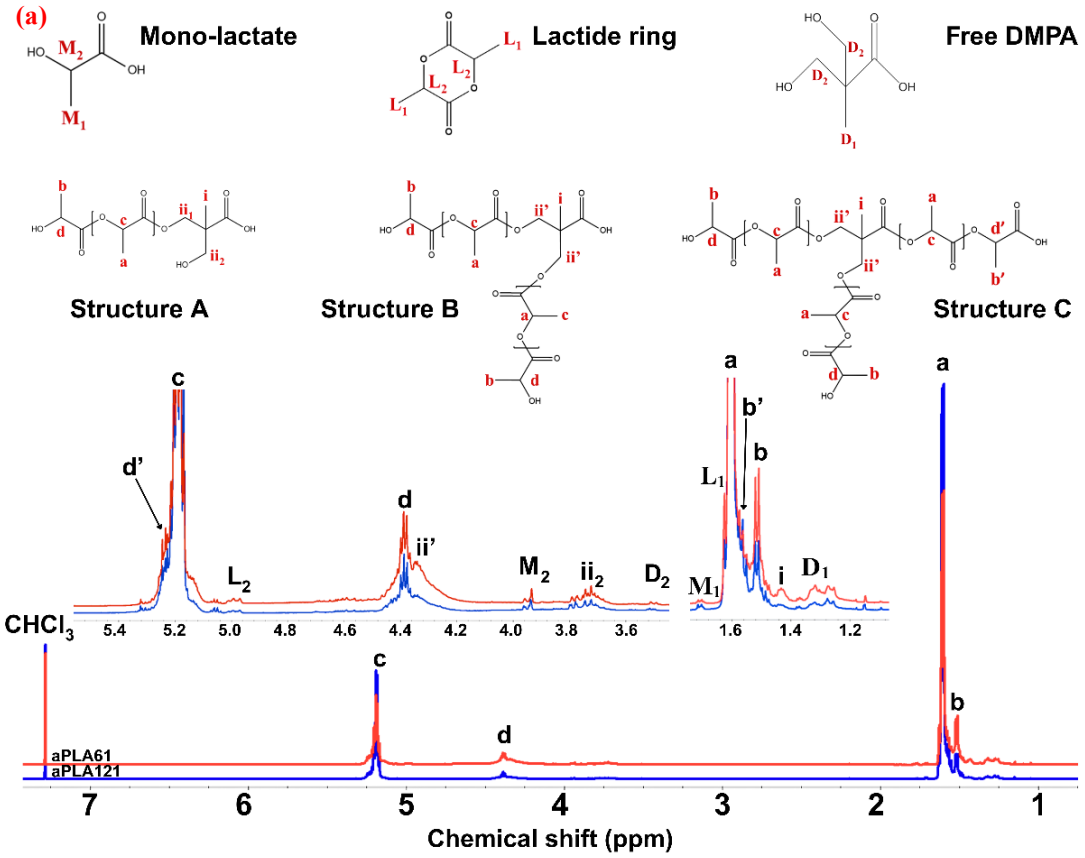

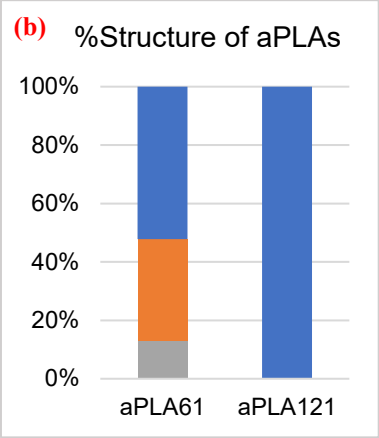

(c)

Sample	Polylactate (%mol)	Monolactate (%mol)	Lactide (%mol)	DMPA (%mol)	$\bar{X}_n$
aPLA61	97.4	0.0	1.9	0.6	3.4
aPLA121	98.7	0.0	1.0	0.3	5.6

Figure 1. (a) ^{1}H-NMR spectra and signal assignments, (b) structural compositions, and (c) composition of lactate sequences of aPLA products generated at 6:1 and 12:1 PLA: DMPA feed contents

Structure A, *Structure B*, and *Structure C.* The lactate sequence length in each structure varies and was classified as mono-lactate and poly-lactate. The average lactate length ($\bar{X}_n$) was calculated using the signals of lactate repeat units at 1.42 ppm (methyl, c) and 4.47 ppm (methine, a), relative to the signals of terminal lactate at 1.51 ppm (terminal CH_3 connected to -OH group, b) and 4.38 ppm (terminal -CH connected to -OH group, d). The corresponding mono-lactate signals were observed at M_1 (1.85 ppm) and M_2 (4.15 ppm). The content of the carboxyl-terminated lactate group in *Structure C* was calculated using the signal b' (1.57 ppm) and d' (5.23 ppm). In contrast, the free DMPA content was monitored using its characteristic signals at D_1 (1.05 ppm) and D_2 (3.51 ppm). The signals at L_1 (1.72 ppm) and L_2 (5.02 ppm) reflect the lactide cyclic dimer co-product. The presence of DMPA in the core structure facilitated structural differentiation through proton shielding effects. Nakayama et al. (2014) characterized the structure of alcoholyzed PLA using a DMPA core unit. The signal i (1.32 ppm) demonstrated the methyl of core DMPA, while ii_1 and ii_2 (3.77 and 3.95 ppm) demonstrated the CH_2 of core DMPA when only one hydroxyl terminal of DMPA reacted (*structure A*), and ii' (4.33 ppm) described the core DMPA in *structures B* and *C* (Nakayama et al., 2014). The shifts in the signals were caused by the OH deshielding the proton from that area. This was attributable to asymmetric structure-induced proton shield variations and could be used to calculate the contents of *Structure A* and COOH-terminals, as well as differentiate between *structures B* and *C* (Nim et al., 2023).

The compositions of the products with different structures are summarized in Figure 1(b). The aPLA121 products exhibited a 100% content of *Structure C*, in which both hydroxyls and the -COOH functionals of DMPA underwent transesterification with PLA chains. *Structure C* was the only product that transforms into a 3-arm branched structure with a COOH terminal. However, at a higher DMPA content, i.e., aPLA61, the *Structure C* content was about 50%, along with *Structures B* and *A*. The high composition of *structure C* in both products was due to the low DMPA content, allowing all of its hydroxyls and carboxylic acid to undergo transesterification with PLA's esters. In addition, *Structures A* and *B* were also produced as the hydroxyl terminal was more readily reactive than the COOH counterpart.

The ^{1}H-NMR quantitative analysis results revealed an inverse relationship between the DMPA feed content and $\bar{X}_n$ of the aPLA products, while the contents of both hydroxyl and carboxylic acid terminals increased proportionally. The poly-lactate content exceeded 97 %mol, with a slight lactide content and free DMPA residue. The $\bar{X}_n$ of 3.4 units/arm was observed for aPLA61, while the number increased to 5.6 for aPLA121. The PDI values obtained from GPC measurements were 2.06 and 2.67. This reflected the presence of a mixture of alcoholyzed products with a large distribution. Nonetheless, this was still suitable for further use without purification (Somnuake et al., 2024b). These smaller-sized lactates possess high relative terminal functional group content, leading to higher polarity, which increases the hydrophilicity when blended with a neat PLA matrix. The content of mono-lactate was negligible due to the relatively high lactate per hydroxyl/carboxylic acid ratios. The lactide and free DMPA contents remained at very low values, reflecting the high transesterification efficiency and suppression of the back-biting reaction to generate lactide rings.

3.2 Morphology of neat PLA and PLA/aPLAs nanofibers

FE-SEM was employed to observe the morphological variations of the electrospun nanofibers fabricated from neat PLA and PLA/aPLA, as shown in Figure 2. The neat PLA

exhibited relatively uniform, rough surface fibers with moderate surface porosity. The porous features were generated when chloroform evaporated in the high-humidity environment (Casasola et al., 2014). When aPLA61 and aPLA121 were added to PLA at 20% (PLA/20aPLA61 and PLA/20aPLA121), the fibers displayed moderate surface roughness with subtle textural irregularities, likely because of the mismatch in polarity between the smaller but more polar aPLAs and the PLA matrix. The morphology of the blend differed from that of neat PLA fibers. The neat PLA showed a rough surface with pore features, but the 20% blend showed an agglomeration of aPLAs with non-porous features. PLA/20aPLA121 possessed small pores and some agglomeration on the surface, reflected by the small pits and particle embossing. As the aPLA content rose to 50%, nanofibers with a significantly pronounced surface smoothness were obtained.

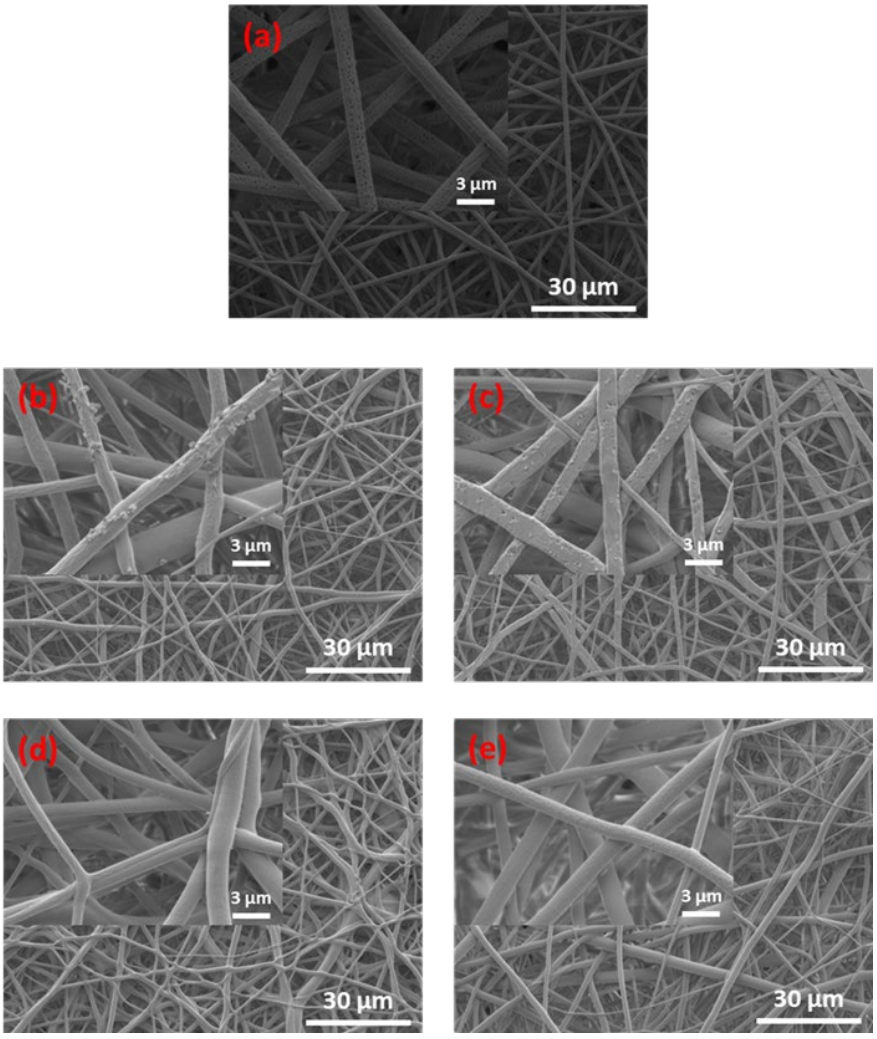

Figure 2. FE-SEM images of electrospun nanofibers of neat PLA (a), PLA/20aPLA61 (b), PLA/20aPLA121 (c), PLA/50aPLA61 (d), and PLA/50aPLA121 (e)

3.3 Chemical structures and crystallinity of neat PLA and PLA/aPLA fiber mats

FTIR spectroscopy was employed to analyze the electrospun fibers' crystallinity, functional groups, and interactions. ATR-FTIR spectra of the samples are compared in Figure 3(a). A weak band at 920 cm^{-1} is characteristic of PLA's α-helix crystalline structure (the C-C stretching coupling with the CH_3 rocking mode), whereas the 955 cm^{-1} band is due to an amorphous region. The overlapped bands of stretching modes can be deconvoluted into three distinct modes at 1753, 1748, and 1721 cm^{-1}, corresponding to the amorphous and crystalline phases of lactate sequences and the acid chain ends. The 3 bands were normalized by an internal standard band, i.e., the -CH_3 bending mode at 1450 cm^{-1}, to quantitatively compare the results across different samples, as shown in Figure 3(b) (Nim & Opaprakasit, 2021). The normalized band area of the acid end groups is compared in Figure 3(c). The value increased with the aPLA composition in the blends and the decreased length of the lactate sequence in the aPLA structure, inherited from the lower PLA: DMPA feed ratios. Given that ATR-FTIR spectroscopy measures the functional groups at the sample's surface, the results imply that the increase in the acid end groups leads to increased hydrophilicity of the sample's surfaces.

The normalized band ratio of the crystalline/amorphous C=O stretching modes was calculated from the 1753/1748 cm^{-1} bands, as shown in Figure 3(d). The results indicate that incorporating smaller-sized aPLAs leads to effective nucleating of the crystallization of the PLA matrix. The blend consisting of aPLA61 showed a higher value than the aPLA121 counterparts at the same blend compositions of 20 or 50%. This is because the smaller-sized aPLA has relatively higher hydroxyl end-groups, which play a key role in hydrogen bonding formation with the C=O groups, inducing crystallization. FTIR spectra measured in ATR mode mainly represent the functional groups at the surface. In contrast, the corresponding transmission spectra show the chemical structures and interactions of the bulk. The band area ratio of specific bands from these two measurements provides information on the distribution of the particular functional groups of the films. The normalized band areas of the α-helix homocrystalline/amorphous band at 920/955 cm^{-1} were calculated. The ratios of the values obtained from the ATR/transmission spectra of different fiber mats are summarized in Figure 3(e). A value of higher than one for all samples indicates a higher density of crystalline content on the surface than inside the fibers. This agrees with SEM results on the migration of smaller-sized aPLA to the fiber's surface, inducing a higher degree of hydrogen bonding and, hence, crystallization (Wang et al., 2013; Lee et al., 2019; Sappayasan, 2019; Nim et al., 2020;).

The XRD pattern of electrospun nanofibers was used to estimate the crystallinity, as shown in Figure 4. Neat PLA showed a strong peak at 16.5°, representing the homocrystallite's (200) or (110) planes, and the 18.8° signal denotes the (203) or (113) planes. After adding aPLAs to the matrix, additional signals were observed at 14.9°, corresponding to the (010) plane, and at 22.1 and 29.0° representing the (210) and (220) planes (Zhang et al., 2005; Opaprakasit et al., 2007; Chen et al., 2014; Phattarateera & Pattamaprom, 2020; Palak et al., 2022; Lv et al., 2023;). This is likely because of the rearrangement of the amorphous phase directly adjacent to the crystalline region. The amorphous halo observed in neat PLA also became weaker while the crystalline signals became more intense and sharper. This reflects an increase in the crystallinity, which is quantitatively calculated in terms of $\%X_c$, as summarized in Figure 5. The results agree with those observed in FTIR quantitative analysis, i.e., the crystallinity increases with the aPLA content. At the same blend composition, the blend consisting of aPLA61 showed higher crystallinity than aPLA121 due to its higher relative hydroxyl and carboxylic acid terminal contents. This confirms that the small-sized oligomers act as a nucleating agent, improving the crystallization of the PLA matrix.

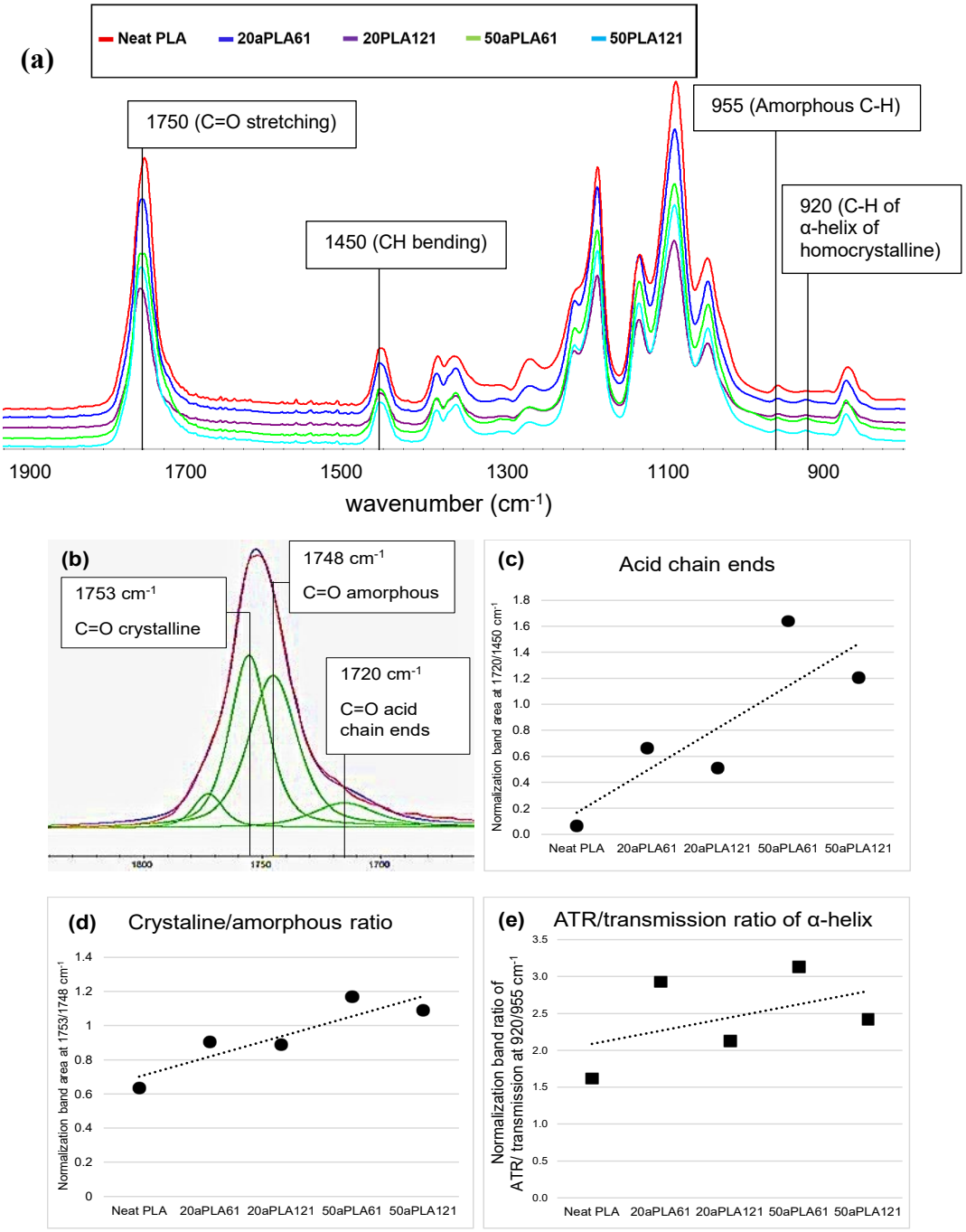

Figure 3. FTIR spectra (a), peak resolve of the overlapped C=O stretching bands (b), normalization band area of acid chain ends at 1720 cm^{-1} (c), ratio of crystalline/amorphous normalization band area of C=O stretching modes (d), and ratio of normalization band area of α -helix homocrystalline/ amorphous band calculated from ATR/transmission spectra (e) of different nanofibers

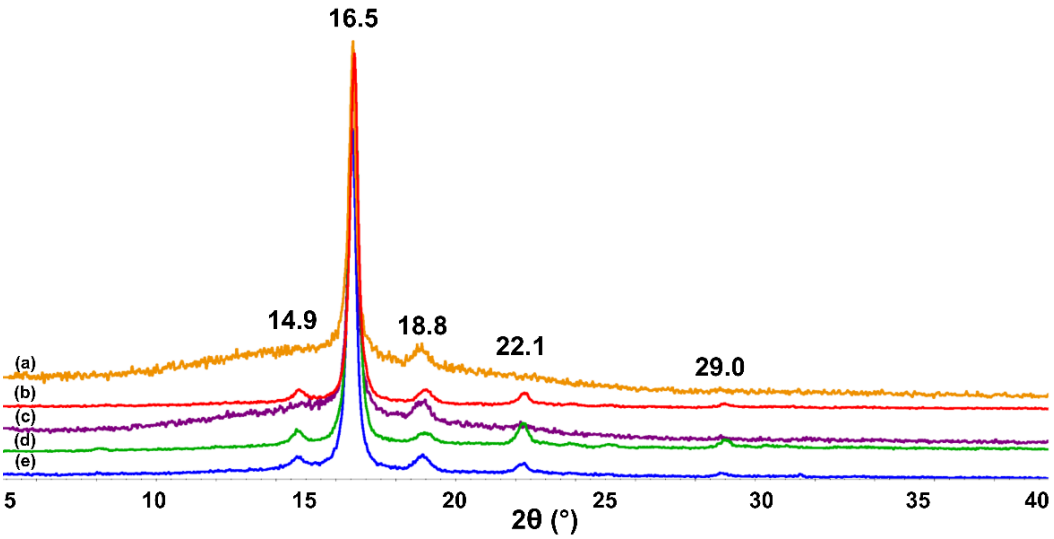

Figure 4. XRD pattern of neat PLA (a), PLA/20aPLA61 (b), PLA/20aPLA121 (c), PLA/50aPLA61 (d), and PLA/50aPLA121 (e)

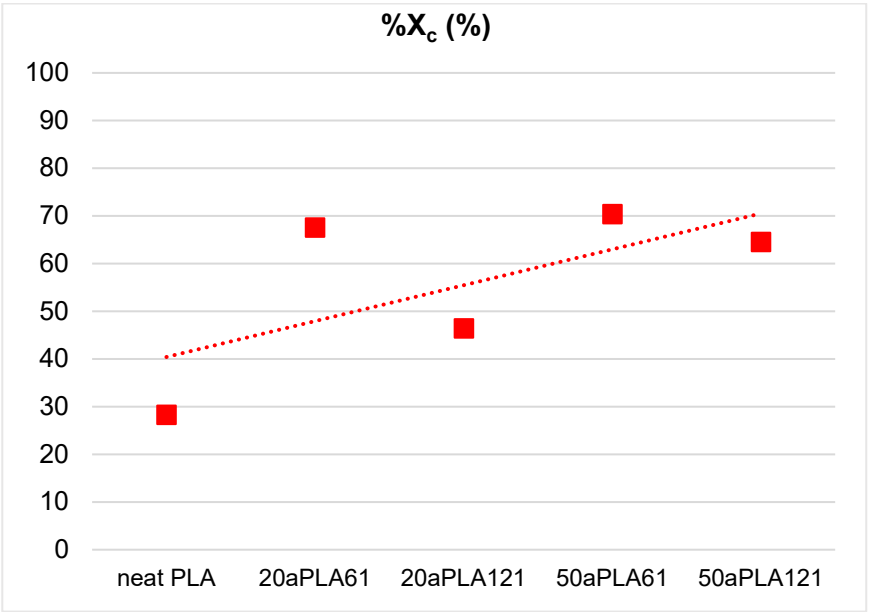

Figure 5. The crystallinity (%X_c) of different electrospun nanofibers, measured by XRD spectroscopy

3.4 Mechanical properties

The mechanical properties of neat PLA and PLA/aPLA nanofiber mats were examined by tensile testing, and the results are summarized in Table 1. The representative stress-strain curves are plotted in Figure 6. The tensile strength of neat PLA decreased when aPLA was introduced because of the diluent effect of the low molecular weight component, which disrupted chain entanglements. At a similar blend composition, the smaller-sized aPLA61 imposed a larger decrease than aPLA121. Young's modulus of all blended fibers was lower than neat PLA, indicating decreased rigidity due to the plasticizing effect. The decrease also depended on the size and composition of aPLA, in which a larger decrease was observed in the blend containing aPLA61 and higher aPLA compositions. Interestingly, an increase in elongation at break was observed in the blends with 20% aPLA content. However, this decreased when the blend content was raised to 50%. This is likely due to the interplay between the plasticizing effect and the induced crystallization from adding aPLA. The optimum condition was observed at 20% blend composition. It was reported that the incorporation of low-molecular-weight PLA could disrupt the orderly arrangement of the polymer chains, creating a free volume that facilitates chain mobility and results in enhanced elongation properties without significant loss of tensile strength at optimal concentrations (Petchsuk et al., 2014; Lv et al., 2023).

Table 1. The mechanical properties of neat PLA and PLA/aPLAs nanofibers as measured in tensile mode

Sample	Tensile Strength (MPa)	Young's Modulus (MPa)	Elongation at Break (%)
Neat PLA	2.5±0.5	80.7±9.1	26.4±3.6
PLA/20aPLA61	1.4±0.1	33.1±12.7	36.7±2.9
PLA/20aPLA121	2.2±0.3	50.0±0.5	47.3±6.2
PLA/50aPLA61	1.4±0.2	75.7±4.9	18.9±2.2
PLA/50aPLA121	2.1±0.4	80.7±9.5	20.2±3.8

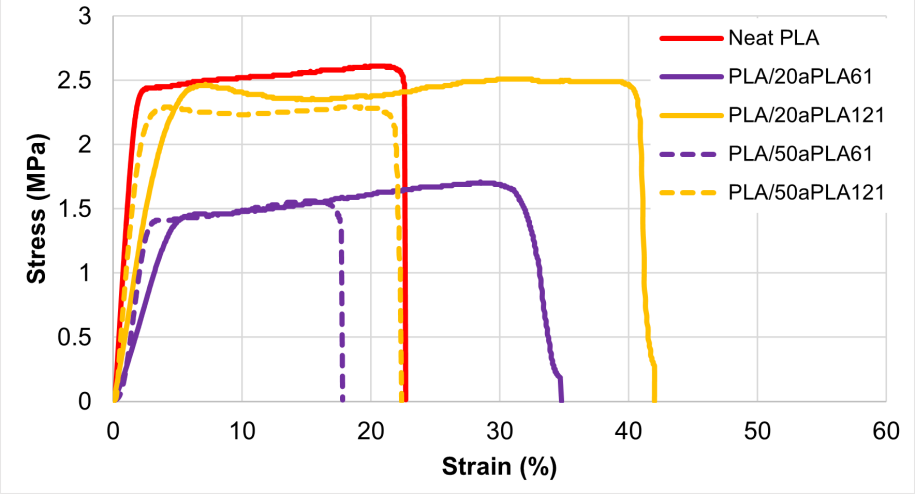

Figure 6. Stress-strain curves of neat PLA and different PLA/aPLAs nanofiber mats

3.5 Hydrophilicity

The hydrophilicity of neat PLA and PLA/aPLA electrospun fiber mats was measured in terms of water contact angle (WCA), and the results are summarized in Table 2 and Figure 7. The neat PLA fiber mat showed a WCA value of 125°±1°, reflecting its hydrophobic nature. All fiber mats containing aPLA exhibited a decrease in the WCA value into the range of 120-122° at an initial water contact time, except for PLA/50aPLA61, which showed a much lower value at 109°±2°. The WCA of the fibers was also monitored as a function of contact time. Due to their improved hydrophilicity, the blends containing aPLA121 showed increased WCA value at 120 s contact time. Interestingly, PLA/aPLA61 blends at both 20 and 50% blend compositions exhibited a faster decrease in the WCA value. The water droplet was entirely absorbed into the fiber mats within 5 and 25 s. This increased hydrophilicity was due to incorporating smaller-sized aPLA with higher polar hydroxyl contents and increasing blend composition (Fuensanta et al., 2020). In our previous work, it was also observed that high contents of both hydroxyl and carboxylic acid terminals in PLA oligomers significantly improved the hydrophilicity of PLA films (Nim et al., 2023). The results indicate that the fibers derived from PLA/aPLA61 blends provide suitable hydrophilicity. The blend containing 20%aPLA61 content showed a balance in mechanical properties and hydrophilicity, making it particularly suitable for tissue engineering applications.

Table 2. The water contact angle (WCA) value of different fiber mats at an initial contact time and after 120 s

Sample	WCA (°)	
	at initial contact	after 120 s
neat PLA	125±1	122±3
PLA/20aPLA61	122±2	N/A*
PLA/20aPLA121	120±2	110±1
PLA/50aPLA61	109±2	N/A*
PLA/50aPLA121	120±1	113±3

*The water droplet was completely absorbed into the fiber mat

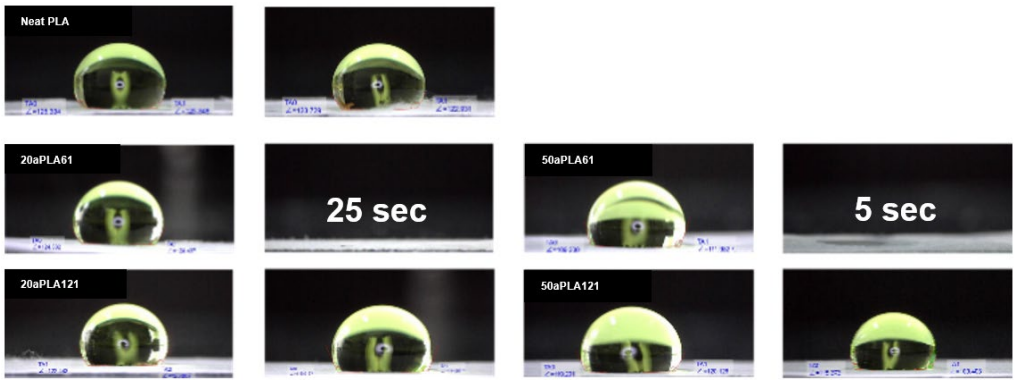

Figure 7. WCA measurement of different nanofibers at an initial dropping time, and the time when the water droplet is completely absorbed, or after 120 s

3.6 Tissue engineering applications

To assess the feasibility of using the electrospun nanofiber mats in biomedical applications, the neat PLA and PLA/20aPLA61 fibers were incubated with L929 cells to examine their cell adhesion and biocompatibility, as shown in Figure 8. The rejection criteria to conclude the test specimen was toxic was that the cells did not appear healthy and showed a change from the normal cell morphology. In contrast, the electrospun nanofibers were non-toxic, with the cells appearing healthy on the nanofibers. Enhanced cell spreading and attachment were observed in the PLA/20aPLA61 nanofibers but not in the neat PLA nanofibers. This improved cellular interaction was attributed to the hydrophilicity of the fibers, particularly terminal carboxyl (-COOH) and hydroxyl (-OH) groups that significantly influenced cell adhesion and proliferation. These functional groups create a more favorable microenvironment by promoting protein adsorption and subsequent cellular attachment through specific integrin-mediated interactions (Benhabbour et al., 2008). Similar results were observed with human dermal fibroblasts and mesenchymal stem cells, where hydrophilic surfaces with exposed -COOH and -OH groups promoted more excellent focal adhesion formation and cytoskeletal organization (Van Tam et al., 2012; Pruchniewski et al., 2025).

Heterogeneous cell adhesive features were observed across different areas of the nanofiber mats of PLA/aPLAs, with characteristic of L929 cells exhibiting adherent growth with morphological heterogeneity. At approximately 7 days after re-plating, the adherent differentiating cells increased to form a confluent layer with small, round-shaped cells interspersed throughout. The image analysis results showed an average of 9 cells attached to the neat PLLA fiber mat. Meanwhile, a much larger number of 560 cells can stay on the fiber's surface of PLA/20aPLA61 mat with standard morphological form and even distribution. This variability was also attributed to subpassages of finite and continuous cell lines, which resulted in phenotypic heterogeneity. Additional factors, such as trypsinization, scraping, and shake-off procedures, can affect cell adhesion morphology, density, and area (Weiss & Blumenson, 1967; Pollard & Walker, 1997; Ma et al., 2012). Lim et al. (2008) reported improved osteoblast proliferation on surfaces with balanced hydrophilicity. The results of our study confirmed that the PLA/aPLAs electrospun fiber scaffolds are non-toxic and effectively mimic the natural extracellular matrix for cell attachment. The enhanced cell-material interactions make these scaffolds significantly superior to neat PLA nanofiber scaffolds for various tissue engineering applications, including skin regeneration, vascular grafts, and neural tissue engineering, where controlled hydrophilicity and surface chemistry are critical design parameters.

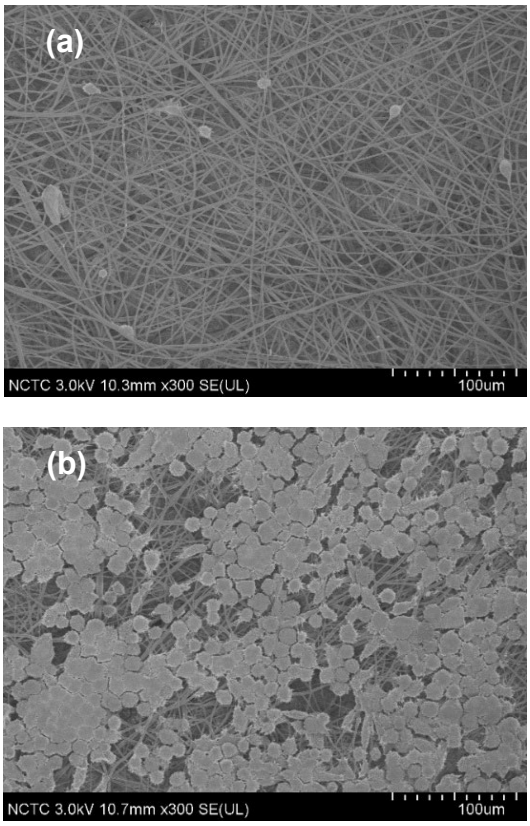

Figure 8. Biocompatibility and cell adhesion morphology of neat PLA and PLA/20aPLA61 nanofiber mats after incubating with L929 cells

4. Conclusions

The acido-alcoholysis of PLA with DMPA successfully produced PLA oligomers (aPLAs) *via* microwave irradiation at a much shorter reaction time, with carboxylic and hydroxyl terminal groups. The products were employed as an effective additive to enhance PLA nanofiber properties significantly. After blending with neat PLA, these aPLAs improved the mechanical properties of the electrospun nanofiber mats, particularly increasing the elongation at break and toughness likely due to their plasticizing effect. Incorporating aPLAs also enhanced the crystallinity of the PLA matrix through their nucleating effect and created fibers with a favorable surface morphology. The blends consisting of 20% aPLA121 exhibited the most balanced mechanical properties, while the aPLA61 blends demonstrated superior hydrophilicity with good mechanical properties. The biocompatibility tests confirmed that the PLA/aPLA nanofibers supported excellent L929 fibroblast cell attachment and growth compared to neat PLA, which was attributed to the increased hydrophilicity and presence of functional carboxylic and hydroxyl groups. These functionalized nanofibers demonstrated significant potential for tissue engineering applications where balanced mechanical properties, controlled hydrophilicity, and cell compatibility are essential. The microwave-assisted alcoholysis approach offers an efficient method for producing functional PLA oligomers with enhanced properties for

producing additives for PLA electrospun nanofibers, which can be applied in tissue engineering and biomedical applications.

5. Acknowledgements

This research was supported by the Thailand Science Research and Innovation Fundamental Fund and the Center of Excellence in Functional Advanced Materials Engineering (CoE FAME), Thammasat University. The doctoral scholarship for the research program from SIIT and Thammasat University, awarded to P.S., is gratefully acknowledged.

6. Authors' Contributions

P.S. was responsible for conceptualization, conducting the experiment, writing an original draft, and editing; A.P. supervised the alcoholysis experiment; M.O. reviewed and edited; P.O. supervised all experiments performed, reviewed, edited, and acquired funding. All authors reviewed the final draft manuscript.

ORCID

Pattara Somnuake https://orcid.org/0009-0001-7915-5843

Atitsa Petchsuk https://orcid.org/0000-0002-3837-0109

Mantana Opaprakasit https://orcid.org/0000-0002-0363-6405

Pakorn Opaprakasit https://orcid.org/0000-0003-1490-8258

7. Conflicts of Interest

The authors declare that they have no known financial conflicts of interest or personal relationships that could have influenced the work reported in this paper.

8. AI Declaration

Grammarly AI and ChatGPT were used for grammar and style suggestions throughout the manuscript, which was reviewed and edited as needed by P.S. and P.O. The authors take full responsibility for the content of the publication.

References

Benhabbour, S. R., Sheardown, H., & Adronov, A. (2008). Cell adhesion and proliferation on hydrophilic dendritically modified surfaces. *Biomaterials*, *29*(31), 4177-4186.

Bhardwaj, N., & Kundu, S. C. (2010). Electrospinning: a fascinating fiber fabrication technique. *Biotechnology Advances*, *28*(3), 325-347.

Casasola, R., Thomas, N. L., Trybala, A., & Georgiadou, S. (2014). Electrospun poly lactic acid (PLA) fibres: Effect of different solvent systems on fibre morphology and diameter. *Polymer*, *55*(18), 4728-4737. https://doi.org/10.1016/j.polymer.2014.06.032

Chen, H.-M., Du, X.-C., Yang, A.-S., Yang, J.-H., Huang, T., Zhang, N., Yang, W., Wang, Y., & Zhang, C.-L. (2014). Effect of graphene oxides on thermal degradation and crystallization behavior of poly(l-lactide). *RSC Advances, 4*(7), 3443-3456. https://doi.org/10.1039/c3ra45480k

Deitzel, J. M., Kleinmeyer, J., Harris, D., & Tan, N. B. (2001). The effect of processing variables on the morphology of electrospun nanofibers and textiles. *Polymer*, *42*(1), 261-272.

Drelich, J., Chibowski, E., Meng, D. D., & Terpilowski, K. (2011). Hydrophilic and superhydrophilic surfaces and materials. *Soft Matter*, *7*(21), 9804-9828. https://doi.org/10.1039/C1SM05849E

Fuensanta, M., Khoshnood, A., & Martín-Martínez, J. M. (2020). Structure–properties relationship in waterborne poly (urethane-urea)s synthesized with dimethylolpropionic acid (DMPA) internal emulsifier added before, during, and after prepolymer formation. *Polymers*, *12*(11), Article 2478. https://doi.org/10.3390/polym12112478

Ganesan, P., Vanaki, S. M., Thoo, K., & Chin, W. (2016). Air-side heat transfer characteristics of hydrophobic and super-hydrophobic fin surfaces in heat exchangers: A review. *International Communications in Heat and Mass Transfer*, *74*, 27-35.

Haider, A., Haider, S., & Kang, I.-K. (2018). A comprehensive review summarizing the effect of electrospinning parameters and potential applications of nanofibers in biomedical and biotechnology. *Arabian Journal of Chemistry*, *11*(8), 1165-1188. https://doi.org/10.1016/j.arabjc.2015.11.015

Hortos, M., Vinas, M., Espino, S., & Bou, J. J. (2019). Influence of temperature on high molecular weight poly(lactic acid) stereocomplex formation. Express Polymer Letters, *13*(2), 123-134. https://doi.org/10.3144/expresspolymlett.2019.12

Huang, C., & Thomas, N. L. (2018). Fabricating porous poly(lactic acid) fibres via electrospinning. *European Polymer Journal*, *99*, 464-476. https://doi.org/10.1016/j.eurpolymj.2017.12.025

Kim, H. H., Kim, M. J., Ryu, S. J., Ki, C. S., & Park, Y. H. (2016). Effect of fiber diameter on surface morphology, mechanical property, and cell behavior of electrospun poly(ε-caprolactone) mat. *Fibers and Polymers*, *17*(7), 1033-1042. https://doi.org/10.1007/s12221-016-6350-x

Lee, K.-M., Park, H., Kim, J., & Chun, D.-M. (2019). Fabrication of a superhydrophobic surface using a fused deposition modeling (FDM) 3D printer with poly lactic acid (PLA) filament and dip coating with silica nanoparticles. *Applied Surface Science*, *467-468*, 979-991. https://doi.org/10.1016/j.apsusc.2018.10.205

Lim, J. Y., Shaughnessy, M. C., Zhou, Z., Noh, H., Vogler, E. A., & Donahue, H. J. (2008). Surface energy effects on osteoblast spatial growth and mineralization. *Biomaterials*, *29*(12), 1776-1784.

López-Fonseca, R., Duque-Ingunza, I., De Rivas, B., Arnaiz, S., & Gutiérrez-Ortiz, J. (2010). Chemical recycling of post-consumer PET wastes by glycolysis in the presence of metal salts. *Polymer Degradation and Stability*, *95*(6), 1022-1028.

Lv, T., Li, J., Liu, L., Huang, S., Li, H., & Jiang, S. (2023). Effects of molecular weight on stereocomplex and crystallization of PLLA/PDLA blends. *Polymer*, *283*, Article 126259. https://doi.org/10.1016/j.polymer.2023.126259

Ma, Z., Hu, Y., Jiang, G., Hou, J., Liu, R., Lu, Y., & Liu, C. (2012). Spontaneous generation of germline characteristics in mouse fibrosarcoma cells. *Scientific Reports*, *2*(1), Article 743. https://doi.org/10.1038/srep00743

Nakayama, Y., Ohmori, T., Tanaka, R., Shiono, T., & Shirahama, H. (2014). Synthesis and properties of polylactide-based poly(ester-urethane)s with ionic groups. *Journal of the Japan Institute of Energy*, *93*(9), 921-925.

Nim, B., Opaprakasit, M., Petchsuk, A., & Opaprakasit, P. (2020). Microwave-assisted chemical recycling of polylactide (PLA) by alcoholysis with various diols. *Polymer Degradation and Stability*, *181*, Article 109363. https://doi.org/10.1016/j.polymdegradstab.2020.109363

Nim, B., & Opaprakasit, P. (2021). Quantitative analyses of products from chemical recycling of polylactide (PLA) by alcoholysis with various alcohols and their applications as healable lactide-based polyurethanes. *Spectrochimica Acta Part A: Molecular and Biomolecular Spectroscopy*, *255*, Article 119684. https://doi.org/10.1016/j.saa.2021.119684

Nim, B., Rahayu, S. S., Thananukul, K., Eang, C., Opaprakasit, M., Petchsuk, A., Kaewsaneha, C., Polpanich, D., & Opaprakasit, P. (2023). Sizing down and functionalizing polylactide (PLA) resin for synthesis of PLA-based polyurethanes for use in biomedical applications. *Scientific Reports*, *13*(1), Article 2284. https://doi.org/10.1038/s41598-023-29496-x

Opaprakasit, P., Opaprakasit, M., & Tangboriboonrat, P. (2007). Crystallization of polylactide and its stereocomplex investigated by two-dimensional Fourier transform infrared correlation spectroscopy employing carbonyl overtones. *Applied Spectroscopy*, *61*(12), 1352-1358.

Palak, H., Güler, E., Nofar, M., & Kayaoğlu, B. K. (2022). Effects of D-lactide content and molecular weight on the morphological, thermal, and mechanical properties of electrospun nanofiber polylactide mats. *Journal of Industrial Textile*s, *51*(2_suppl), 3030S-3056S. https://doi.org/10.1177/15280837221090260

Pang, X., Zhuang, X., Tang, Z., & Chen, X. (2010). Polylactic acid (PLA): research, development and industrialization. *Biotechnology Journal*, *5*(11), 1125-1136. https://doi.org/10.1002/biot.201000135

Petchsuk, A., Buchatip, S., Supmak, W., Opaprakasit, M., & Opaprakasit, P. (2014). Preparation and properties of multi-branched poly (D-lactide) derived from polyglycidol and its stereocomplex blends. *Express Polymer Letters*, *8*(10), 779-789. https://doi.org/10.3144/expresspolymlett.2014.80

Phattarateera, S., & Pattamaprom, C. (2020). The effect of different acrylic-based rubbers on the crystallization behavior of PLA/PDLA stereocomplex. *Journal of Polymers and the Environment*, *28*(6), 1592-1600. https://doi.org/10.1007/s10924-020-01707-w

Pollard, J. W., & Walker, J. M. (1997). *Basic cell culture protocols*. 2nd Ed. Human Press.

Promnil, S., Numpaisal, P.-O., & Ruksakulpiwat, Y. (2021). Effect of molecular weight on mechanical properties of electrospun poly (lactic acid) fibers for meniscus tissue engineering scaffold. *Materials Today: Proceedings*, *47*(Part 12), 3496-3499. https://doi.org/10.1016/j.matpr.2021.03.504

Pruchniewski, M., Strojny-Cieślak, B., Nakielski, P., Zawadzka, K., Urbańska, K., Rybak, D., Zakrzewska, A., Grodzik, M., & Sawosz, E. (2025). Electrospun poly-(L-lactide) scaffold enriched with GO-AuNPs nanocomposite stimulates skin tissue reconstruction via enhanced cell adhesion and controlled growth factors release. *Materials and Design*, *251*, Article 113713. https://doi.org/10.1016/j.matdes.2025.113713

Sappayasan, M. (2019). *Biocomposite scaffolds based on polylactide and chitin/chitosan from fungi extract for tissue engineering applications*. [Master of Engineering thesis, Thammasat University]. TU Digital Collections. https://digital.library.tu.ac.th/tu_dc/frontend/Info/item/dc:175891

Shafrin, E. G., & Zisman, W. A. (1960). Constitutive relations in the wetting of low energy surfaces and the theory of the retraction method of preparing monolayers. *The Journal of Physical Chemistry*, *64*(5), 519-524. https://doi.org/10.1021/j100834a002

Sinha, V., Patel, M. R., & Patel, J. V. (2010). PET waste management by chemical recycling: a review. *Journal of Polymers and the Environment*, *18*(1), 8-25.

Somnuake, P. (2021). *Electrospun nanofibers of polylactide (PLA) stereocomplex with super-hydrophobic surfaces for potential use in facial mask and biomedical applications*. [Master of Engineering thesis, Thammasat University]. TU Digital Collections. https://digital.library.tu.ac.th/tu_dc/frontend/Info/item/dc:272969

Somnuake, P., Petchsuk, A., Opaprakasit, M., & Opaprakasit, P. (2024a). Sizing down of polylactide (PLA) by 2,2-bis(hydroxymethyl)propionic acid for toughening and enhancing the hydrophilicity of PLA cast films. In *The 6th International Conference on Smart Materials and Nanotechnology (SMARTMAT2024)*, Chiangmai.

Somnuake, P., Puttawong, P., & Wacharawichanant, S. (2024b). Morphology and properties of poly (lactic acid)/ethylene propylene diene monomer blends with micro-cellulose fibers from paper pulp. *Advances in Science and Technology*, *150*, 3-10. https://doi.org/10.4028/p-D4crNi

Van Tam, J. K., Uto, K., Ebara, M., Pagliari, S., Forte, G., & Aoyagi, T. (2012). Mesenchymal stem cell adhesion but not plasticity is affected by high substrate stiffness. *Science and Technology of Advanced Materials*, *13*(6), Article 064205. https://doi.org/10.1088/1468-6996/13/6/064205

Wacharawichanant, S., Wimonsupakit, N., & Kuhaudomlap, S. (2018). Comparison of morphology and mechanical properties of polyoxymethylene/cellulose and poly(lactic acid)/cellulose composites. *Materials Science Forum*, *916*, 19-23. https://doi.org/10.4028/www.scientific.net/MSF.916.19

Wang, D. K., Varanasi, S., Fredericks, P. M., Hill, D. J., Symons, A. L., Whittaker, A. K., & Rasoul, F. (2013). FT-IR characterization and hydrolysis of PLA-PEG-PLA based copolyester hydrogels with short PLA segments and a cytocompatibility study. *Journal of Polymer Science Part A: Polymer Chemistry*, *51*(24), 5163-5176.

Wang, F., Liang, C., Zhang, Y., & Zhang, X. (2017). Defrosting performance of superhydrophobic fin-tube heat exchanger. *Applied Thermal Engineering*, *113*, 229-237.

Weiss, L., & Blumenson, L. E. (1967). Dynamic adhesion and separation of cells in vitro II. Interactions of cells with hydrophilic and hydrophobic surfaces. *Journal of cellular Physiology*, *70*(1), 23-32.

Zhang, J., Duan, Y., Sato, H., Tsuji, H., Noda, I., Yan, S., & Ozaki, Y. (2005). Crystal modifications and thermal behavior of poly (L-lactic acid) revealed by infrared spectroscopy. *Macromolecules*, *38*(19), 8012-8021.